J|A|C|S
ARTICLES
Published on Web 03/21/2002

Theoretical Study of the Mechanism of Alkane Hydroxylation and Ethylene Epoxidation Reactions Catalyzed by Diiron Bis-oxo Complexes. The Effect of Substrate Molecules

Djamaladdin G. Musaev,*,† Harold Basch,*,†,‡ and Keiji Morokuma*,†

Contribution from the Cherry L. Emerson Center for Scientific Computation and Department of Chemistry, Emory University, Atlanta, Georgia 30322, and Department of Chemistry, Bar Ilan University, Ramat Gan 52900, Israel

Received November 29, 2001

Abstract: The hybrid density functional method B3LYP was used to study the mechanism of the hydrocarbon (methane, ethane, methyl fluoride, and ethylene) oxidation reaction catalyzed by the complexes *cis*-$(H_2O)(NH_2)Fe(\mu\text{-}O)_2(\eta^2\text{-}HCOO)_2Fe(NH_2)(H_2O)$, **I**, and *cis*-$(HCOO)(Imd)Fe(\mu\text{-}O)_2(\eta^2\text{-}HCOO)_2Fe(Imd)(HCOO)$ (Imd = Imidazole), **I_m**, the "small" and "medium" model of compound **Q** of the methane monooxygenase (MMO). The improvement of the model from "small" to "medium" did not change the qualitative conclusions but significantly changed the calculated energetics. As in the case of methane oxidation reported by the authors previously, the reaction of all the substrates studied here is shown to start by coordination of the substrate molecule to the bridging oxygen atom, O^1 of **I**, an Fe(IV)-Fe(IV) complex, followed by the H-atom abstraction at the transition state **III** leading to the bound hydroxy alkyl intermediate **IV** of Fe(III)-Fe(IV) core. **IV** undergoes a very exothermic coupling of alkyl and hydroxy groups to give the alcohol complex **VI** of Fe(III)-Fe(III) core, from which alcohol dissociates. The H^b-atom abstraction (or C−H bond activation) barrier at transition state **III** is found to be a few kcal/mol lower for C_2H_6 and CH_3F than for CH_4. The calculated trend in the H^b-abstraction barrier, CH_4 (21.8 kcal/mol) > CH_3F (18.8 kcal/mol) ≥ C_2H_6 (18.5 kcal/mol), is consistent with the C−H^b bond strength in these substrates. Thus, the weaker the C−H^b bond, the lower is the H^b-abstraction barrier. It was shown that the replacement of a H-atom in a methane molecule with a more electronegative group tends to make the H^b-abstraction transition state less "reactant-like". In contrast, the replacement of the H-atom in CH_4 with a less electronegative group makes the H^b-abstraction transition state more "reactant-like". The epoxidation of ethylene by complex **I** is found to proceed without barrier and is a highly exothermic process. Thus, in the reaction of ethylene with complex **I** the only product is expected to be ethylene oxide, which is consistent with the experiment.

I. Introduction

Methane monooxygenase (MMO) is an enzyme that catalyzes the oxidation of a wide variety of substrates including methane molecule and olefins.[1−5] During these reactions the O−O bond of O_2 is cleaved, followed by reduction of one of the O atoms to water, and incorporation of the second one into the substrate. X-ray crystallographic studies of the soluble MMO (sMMO) enzyme from both *Methylococcus capsulatus* (Bath)[6] and *Methylosinus trichosporium* OB3b[7] have demonstrated that it contains three proteins: iron-containing hydroxylase (MMOH), a reductase (MMOR), and a regulatory or coupling component, protein B (MMOB). Although each of these three proteins is required for efficient substrate hydroxylation coupled to NADH oxidation, it has been established that the diferrous state of hydroxylase ($MMOH_{red}$) is the only one capable of reacting with dioxygen and initiating the catalytic cycle. It reacts with O_2 and forms a metastable compound **O**, which spontaneously converts to compound **P**. Compound **P** easily transforms to compound **Q**, which was proposed to contain two antiferromagnetically coupled high-spin Fe^{IV} centers. EXAFS and spectroscopic studies[8,9] of compound **Q**, which was trapped from *M. trichosporium* OB3b and *M. capsulatus*, have demonstrated

* To whom correspondence should be addressed. E-mail: morokuma@emory.edu.
† Emory University.
‡ Bar Ilan University.

(1) (a) Feig, A. L.; Lippard, S. *Chem. Rev.* **1994**, *94*, 759. (b) Liu, K. E.; Lippard, S. *J. Adv. Inorg. Chem.* **1995**, *42*, 263.
(2) Valentine, A. M.; Stahl, S. S.; Lippard, S. J. *J. Am. Chem. Soc.* **1999**, *121*, 3876 and references therein.
(3) Wallar, B. J.; Lipscomb, J. D. *Chem. Rev.* **1996**, *96*, 2625 and references therein.
(4) Merkx, M.; Kopp, D. A.; Sazinsky, M. H.; Blazyk, J. L.; Muller, J.; Lippard, S. J. *Angew. Chem., Int. Ed.* **2001**, *40*, 2782.
(5) Solomon, E.; Brunold, T. C.; Davis, M. I.; Kemsley, J. N.; Lee, S.-K.; Lehnert, N.; Neese, F.; Skulan, A. J.; Yang, Y.-S.; Zhou, J. *Chem. Rev.* **2000**, *100*, 235 and references therein.
(6) (a) Rosenzweig, A. C.; Fredrick, C. A.; Lippard, S. J.; Nordlung, P. *Nature* **1993**, *366*, 537. (b) Rosenzweig, A. C.; Nordling, P.; Takahara, P. M.; Fredrick, C. A.; Lippard, S. *Chem. Biol.* **1995**, *2*, 409.
(7) Elango, N.; Radhakrishman, R.; Froland, W. A.; Waller, B. J.; Earhart, C. A.; Lipscomb, J. D.; Ohlendorf, D. H. *Protein Sci.* **1997**, *6*, 556. (b) Nesheim, J. C.; Lipscomb, J. D. *Biochemistry* **1996**, *35*, 10240 and references therein.
(8) Wilkinson, E. C.; Dong, Y.; Zang, Y.; Fujii, H.; Fraczkiewicz, R.; Fraczkiewicz, G.; Czernuszewicz, R. S.; Que, L., Jr. *J. Am. Chem. Soc.* **1998**, *120*, 955.
(9) Shu, L.; Nesheim, J. C.; Kauffmann, K.; Munck, E.; Lipscomb, J. D.; Que, L., Jr. *Science* **1997**, *275*, 515.

that it has a diamond core $(Fe^{IV})_2(\mu\text{-}O)_2$ structure with one short (1.77 Å) and one long (2.05 Å) Fe−O bond per Fe atom and a short Fe−Fe distance of 2.46 Å. Previously[3,6,7] it was shown that the Fe ions are bridged by two bidentate Glu γ-carboxylates. In addition, each Fe ion is coordinated by one His and one monodentate Glu carboxylate.

The mechanism by which compound **Q** reacts with substrates is the key to the monooxygenase chemistry. Although the reaction of **Q** with substrates may involve both binding and reaction steps,[15] no intermediates have been detected in the reaction step itself. Despite that, in the literature,[1−5,10,11] various mechanisms for the reaction of **Q** with a methane molecule (alkane, in general) have been proposed, which can be divided into three different classes: (1) radical, (2) nonradical, and (3) carbocation-type mechanisms. The radical mechanism starts with abstraction of the hydrogen atom from the substrate to form **QH** (hydroxyl bridged **Q** compound) and free alkyl radical, while the nonradical mechanism implies a concerted pathway, occurring via a four-center transition state and leading to "hydrido-alkyl-**Q**" compound. The latest experimental studies[12,13] show that the reaction mechanism could even be more complicated and may involve carbocation-type species instead of alkyl radicals. Because the lifetime of the formed intermediates is very short, the use of the spectroscopic methods for their identification is very problematic, and more indirect methods are needed.

Furthermore, extensive studies of the hydrocarbon hydroxylation by MMO for different substrates show a surprisingly large diversity. For example, kinetic isotope effect studies for decay of compound **Q** show a large isotope effect for CH_4 versus CD_4, while no kinetic isotope effect was observed for C_2H_6 versus C_2D_6 (and many other large substrates).[2,4,14] These results indicate that the substrate-binding step could be rate-determining for the decay of **Q** for these substrates rather than the C−H bond cleavage.[15] Intramolecular KIEs for methane and chiral ethane obtained by studying product ratios show a large substrate difference, which could indicate the presence of a complex mechanism for the decay of compound **Q** and/or substrate oxidation by pathways other than the decay of **Q**.[14,16] Further studies indicate that not only different substrates may react with **Q** in different ways, but that they may also react with different oxygen intermediates.[4] For example, it is well established that methane hydroxylation occurs on compound **Q**. However, there are conflicting evidences about the possible reactive oxygen intermediates for the olefin epoxidation processes. Lippard and co-workers have suggested that most likely the reactive species for the propene epoxidation process is the peroxo complex **P** formed upon coordination of O_2 molecule to the $MMOH_{red}$, for example, before the O−O cleavage and **Q** formation processes,[2,4] while latest data of Lipscomb and co-workers did not support this conclusion.[15] Thus, these and many other experimental findings show the high complexity of the mechanism of hydrocarbon hydroxylation by MMO, which could change by changing substrate molecules.

To provide some insight into the reaction mechanism of compound **Q** with different hydrocarbons, comprehensive computational approaches could be extremely useful. Previously, we[10,17−22] and other[23−25] theoretical groups have studied the mechanism of methane hydroxylation by compound **Q**. As we pointed out in 1999[17] and was supported later,[25a] methane oxidation by compound **Q** seems to occur via the "bound radical" mechanism. However, the effects of substrate molecule on this process, as well as the mechanism of olefin epoxidation reaction, still remain unsolved. Therefore, in this paper we discuss the mechanism of the reaction of intermediate **Q** with methane (previously described[17,18]), methyl fluoride, and ethane (with general formula of XCH_3, where X = H, F, and CH_3, respectively), as well as with ethylene. The reactions of **P** compound ($MMOH_{peroxo}$) with ethylene will not be treated here and will be a topic of our future study.

Thus, the purpose of this paper is to study the mechanism of the reaction:

$$\{Fe_2(\mu\text{-}O)_2\}_{\mathbf{Q}} + XCH_3 \rightarrow \{Fe_2(\mu\text{-}O)(HOCXH_2)\}\{Fe_2(\mu\text{-}O)\} + HOCXH_2 \quad (1)$$

and

$$\{Fe_2(\mu\text{-}O)_2\}_{\mathbf{Q}} + C_2H_4 \rightarrow \{Fe_2(\mu\text{-}O)(HOC_2H_3)\} \rightarrow \{Fe_2(\mu\text{-}O)\} + HOC_2H_3 \quad (2a)$$

$$\rightarrow \{Fe_2(\mu\text{-}O)(OC_2H_4)\} \rightarrow \{Fe_2(\mu\text{-}O)\} + OC_2H_4 \quad (2b)$$

using the quantum chemical methods.

However, as was mentioned in our previous papers,[10,17−22] to conduct quantum chemical research, first one has to answer several nontrivial questions. First, one has to choose a reasonable model for the intermediate **Q** incorporating all available

(10) (a) Morokuma, K.; Musaev, D. G.; Vreven, T.; Basch, H.; Torrent, M.; Khoroshun, D. V. *IBM J. Res. Dev.* **2001**, *45*, 367. (b) Torrent, M.; Musaev, D. G.; Basch, H.; Morokuma, K. *J. Comput. Chem.* **2001**, in press.
(11) Steinman, A. A. *J. Biol. Inorg. Chem.* **1998**, *3*, 325.
(12) Valentine, A. M.; Wilkinson, B.; Liu, K. E.; Komar-Panicucci, S.; Priestley, N. D.; Williams, P. G.; Mirimoto, H.; Floss, H. G.; Lippard, S. J. *J. Am. Chem. Soc.* **1997**, *119*, 1818.
(13) Choi, S. Y.; Eaton, P. E.; Kopp, D. A.; Lippard, S. J.; Newcomb, M.; Shen, R. *J. Am. Chem. Soc.* **1999**, *121*, 12198.
(14) Nesheim, J. C.; Lipscomb, J. D. *Biochemistry* **1996**, *35*, 10240.
(15) Brazeau, B. J.; Lipscomb, J. D. *Biochemistry* **2000**, *39*, 13503.
(16) Priestley, N. D.; Floss, H. G.; Froland, W. A.; Lipscomb, J. D.; Williams, P. G.; Morimoto, H. *J. Am. Chem. Soc.* **1992**, *114*, 7561.
(17) Basch, H.; Mogi, K.; Musaev, D. G.; Morokuma, K. *J. Am. Chem. Soc.* **1999**, *121*, 7249.
(18) Basch, H.; Musaev, D. G.; Mogi, K.; Morokuma, K. *J. Phys. Chem. A* **2001**, *105*, 3615.
(19) Torrent, M.; Musaev, D. G.; Morokuma, K.; Basch, H. *J. Phys. Chem. B* **2001**, *105*, 4453
(20) Torrent, M.; Mogi, K.; Basch, H.; Musaev, D. G.; Morokuma, K. *J. Phys. Chem. B* **2001**, *105*, 8616.
(21) Basch, H.; Musaev, D. G.; Morokuma, K. *J. Phys. Chem. B* **2001**, *105*, 8452.
(22) Torrent, M.; Musaev, D. G.; Morokuma, K. *J. Phys. Chem. B* **2001**, *105*, 322.
(23) (a) Yoshizawa, K.; Hoffmann, R. *Inorg. Chem.* **1996**, *35*, 2409. (b) Yoshizawa, K.; Yamabe, T.; Hoffmann, R. *New J. Chem.* **1997**, *21*, 151. (c) Yoshizawa, K.; Ohta, T.; Yamabe, T.; Hoffmann, R. *J. Am. Chem. Soc.* **1997**, *119*, 12311. (d) Yoshizawa, K. *J. Biol. Inorg. Chem.* **1998**, *3*, 318. (e) Yoshizawa, K.; Shiota, Y.; Yamabe, T. *Chem.-Eur. J.* **1997**, *3*, 1160. (f) Yoshizawa, K.; Shiota, Y.; Yamabe, T. *J. Am. Chem. Soc.* **1998**, *120*, 564. (g) Yoshizawa, K.; Shiota, Y.; Yamabe, T. *Organometallics* **1998**, *17*, 2825. (h) Yoshizawa, K. *J. Inorg. Biochem.* **2000**, *78*, 23. (i) Yoshizawa, K.; Ohta, T.; Yamabe, T. *Bull Chem. Soc. Jpn.* **1998**, *71*, 1899, 80862. (j) Yoshizawa, K.; Yokomichi, Y.; Shiota, Y.; Ohta, T.; Yamabe, T. *Chem. Lett.* **1997**, 587.
(24) (a) Siegbahn, P. E. M.; Crabtree, R. H. *J. Am. Chem. Soc.* **1997**, *119*, 3103. (b) Siegbahn, P. E. M.; Crabtree, R. H.; Nordlund, P. *J. Biol. Inorg. Chem.* **1998**, *3*, 314. (c) Siegbahn, P. E. M. *J. Am. Chem. Soc.* **1998**, *120*, 8417. (d) Siegbahn, P. E. M.; Eriksson, L.; Himo, F.; Pavlov, M. *J. Phys. Chem. B* **1998**, *102*, 10622. (e) Siegbahn, P. E. M. *Inorg. Chem.* **1999**, *38*, 2880. (f) Siegbahn, P. E. M. *J. Biol. Inorg. Chem.* **2001**, *6*, 27. (g) Siegbahn, P. E. M.; Blomberg, M. R. A. *Annu. Rev. Phys. Chem.* **1999**, *50*, 221.
(25) (a) Dunietz, B. D.; Beachy, M. D.; Cao, Y.; Whittington, D. A.; Lippard, S. J.; Friesner, R. A. *J. Am. Chem. Soc.*, **2000**, *122*, 2828. (b) Gherman, B. F.; Dunietz, B. D.; Whittington, D. A.; Lippard, S. J.; Friesner, R. A. *J. Am. Chem. Soc.* **2001**, *123*, 3836.

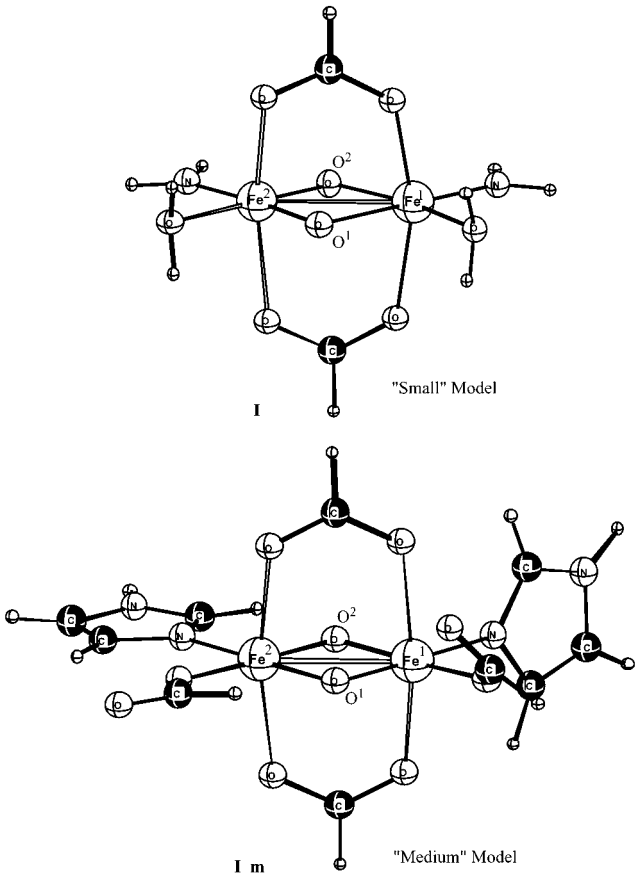

Figure 1. The model systems used in the paper.

experiment findings. According to our previous studies the smallest reasonable model of compound **Q** satisfying all experimental conditions is *cis*-$(H_2O)(NH_2)Fe(\mu\text{-}O)_2(\eta^2\text{-}HCOO)_2$-$Fe(NH_2)(H_2O)$, **I** (see Figure 1). The particular choice of this model has been explained in detail previously.[10] This model was successfully used[17,18] to describe the reaction of **Q** with CH_4. One should note that recently Friesner and co-workers[25a] have published their studies of the mechanism of the C−H activation reaction {**Q** + CH_4} using a very large model including about 100 atoms. Their findings and conclusions are nearly the same as those of our previous paper that used the same small model, **I**. Also, our recent studies[26] using an extremely large model including about 1000 atoms unambiguously demonstrated the usefulness of our small model in describing the ligand environment of the active sites of $MMOH_{ox}$ and $MMOH_{red}$. Despite that, we would like to validate our small model **I** once again by recalculating the reaction mechanism of the compound **Q** with CH_4 using a medium size model, *cis*-$(HCOO)(Imd)Fe(\mu\text{-}O)_2(\eta^2\text{-}HCOO)_2Fe(Imd)(HCOO)$ (Imd = imidazole), **I_m** (see Figure 1), which we previously[22] used successfully in a study of "1,2-carboxylate" shift in $MMOH_{red}$.

Other important questions are the spin state of the system and the choice of adequate computational methods. Spectroscopic studies show that compound **Q** is diamagnetic and contains two antiferromagnetic coupled high-spin Fe^{IV} atoms.[8,9] **Q** is EPR silent, and the exchange coupling J constant is found to be >60 cm^{-1}. Use of multideterminant methods, which are the most appropriate methods for such systems, is extremely expensive and impractical for such large compounds. On the other hand, in the less-expensive single-determinant methods (like DFT) it is difficult to represent the open-shell low spin coupling ($2S + 1 = 0$) of the two paramagnetic metal centers, each having the multiplicity $2S + 1 = 5$ (Fe(IV), d^4) or 6 (Fe(III), d^5). Here exist two alternatives. The first is the broken symmetry approach developed by Yamaguchi et al.[27] and Noodleman[28] where the Heisenberg exchange coupling constants were calculated from the energy difference of the high spin state and the broken symmetry low spin state using spin-projection methods. The second one is to perform the spin-unrestricted open-shell single-determinant calculations for ferromagnetically coupled high spin states when the magnitude of the spin coupling between the two metal centers is not strong. As previously discussed,[10] the second approach which retains the proper spins on the individual metal (Fe) atoms is more practical. Therefore, below we performed spin-unrestricted open-shell single-determinant DFT calculations for ferromagnetically coupled high spin states such as ^{9}A and ^{11}A (see section II for more detail).

As seen in Figure 1, the substrate molecule may coordinate and react with the bridging oxygen atoms O^1 and O^2 of model **I** (or **I_m**) located on the H_2O (or HCOO) and NH_2 (or Imd)-sides, respectively. These two pathways will be called the O-side and N-side pathways, respectively. According to experimental data,[1,3,5] the only valid pathway is the coordination of the substrate from the O-side because of the existence of the substrate coordination pocket; the coordination of substrate from the N-side is sterically hindered and not available. Despite that, in our previous papers[10,17,18] we have studied both the O-side and the N-side pathways, and have found that the N-side pathway is intrinsically more reactive. However, to be consistent with experimental studies, in the present paper we will discuss only the O-side pathway.

II. Computational Procedure

As mentioned above, in this paper we use the small, *cis*-$(H_2O)(NH_2)$-$Fe(\mu\text{-}O)_2(\eta^2\text{-}HCOO)_2Fe(NH_2)(H_2O)$, **I**, and medium, *cis*-$(HCOO)(Imd)$-$Fe(\mu\text{-}O)_2(\eta^2\text{-}HCOO)_2Fe(Imd)$ (HCOO), **I_m** (see Figure 1), models. Because the magnitude of the antiferromagnetic spin coupling between the two Fe-centers of the diamagnetic compound **Q** is not strong (see above discussion), we expect that the mechanism of reactions 1 and 2 is not much influenced by the antiferromagnetic nature of the complex. Therefore, we performed spin-unrestricted open-shell single-determinant calculations for ferromagnetically coupled high spin states with multiplicities of $2M_S + 1 = 9$ and 11, ^{9}A and ^{11}A, respectively. In these calculations, we used the hybrid density functional method, B3LYP,[29] in conjunction with the Stevens−Basch−Krauss (SBK) effective core potentials (ECP) and the standard split-valence 31G, CEP-31, and (8s8p6d/4s4p3d) basis sets for H (C, O, and N) and Fe atoms, respectively[30] (below, we call it the SBK basis set), for geometry optimization. The energies were recalculated at the B3LYP/SBK optimized geometries with two polarization basis sets, SBK($+d_{C,O}$) and SBK($+d_{C,N,O}$), at the B3LYP level; SBK($+d_{C,O}$) is the SBK basis set

(26) Torrent, M.; Vreven, T.; Musaev, D. G.; Morokuma, K.; Farkas, O.; Schlegel, H. B. *J. Am. Chem. Soc.* **2002**, *124*, 192.

(27) (a) Yamaguchi, K.; Fukui, H.; Fueno, T. *Chem. Lett.* **1986**, *4*, 525. (b) Yamaguchi, K.; Jensen, F.; Dorigo, A.; Houk, K. N. *Chem. Phys. Lett.* **1988**, *149*, 537.

(28) Noodleman, L. *J. Chem. Phys.* **1981**, *74*, 5737.

(29) (a) Becke, A. D. *Phys. Rev. A* **1988**, *38*, 3098. (b) Becke, A. D. *J. Am. Chem. Soc.* **1993**, *115*, 1372. (c) Becke, A. D. *J. Chem. Phys.* **1993**, *98*, 5648. (d) Lee, C.; Yang, W.; Parr, R. G. *Phys. Rev. B* **1988**, *37*, 785.

(30) (a) Stevens, W. J.; Basch, H.; Krauss, M. *J. Chem. Phys.* **1984**, *81*, 6026. (b) Stevens, W. J.; Krauss, M.; Basch, H.; Jasien, P. G. *Can. J. Chem.* **1992**, *70*, 612.

augmented by a set of polarization d-functions on all oxygen (α_O = 0.85) and carbon (α_C = 0.75) atoms. The largest basis set SBK(+$d_{C,N,O}$) adds further to SBK(+$d_{C,O}$) a set of polarization d-functions (α_N = 0.80) on the N atoms. Note that in our previous calculations[17,18] we used the same SBK basis set for the geometry optimizations, but a slightly different SBK(+$d_{C,O}$) basis set for the energy calculations, where polarization d-functions were added only on the methane carbon as well as all oxygen atoms, except those on two terminal water molecules, which below we call SBK(+$d_{C,O}'$). Previously, the B3LYP method with a double-ζ quality basis set has been shown to be quite reliable both in geometry and in energy.[31]

All calculations were performed using the Gaussian98 package.[32] Second derivative (frequency) calculations were carried out for all equilibrium and transition state structures. In addition, to confirm the nature of the calculated TS2 structures, quasi-IRC (intrinsic reaction coordinate) calculations were carried out in the following manner. The geometry of the transition state was at first shifted, both toward the reactant and toward the product side, and then was released for equilibrium optimization. In this manner, each transition state was "connected" to the reactant and the product of the respective step. For the TS1 structures, analytical IRC calculations were carried out to connect reactants and products. The energies given here and discussed below do not include zero point energy correction (ZPC). Below, we discuss the energetics calculated at the B3LYP/SBK(+$d_{C,O}$) and B3LYP/SBK(+$d_{C,N,O}$) levels, while B3LYP/SBK energies are given in the Supporting Information (Tables S1 and S2).

III. Results and Discussions

A. Comparison of "Small" and "Medium" Model Studies for the Reaction of Q with CH_4. As mentioned above, previously the reaction mechanism of the complex **Q** with the molecule of methane has been actively studied by several theoretical groups including us. In general, the obtained results are qualitatively the same, while the calculated energetics differ somewhat depending on the methods and models used. Briefly, by using the "small" model **I**, and B3LYP/SBK and B3LYP/SBK(+$d_{C,O}'$) methods for the geometry optimization and energetics, respectively, we[17,18] previously found the following:

(1) The reaction of complex **I** with a molecule of methane proceeds via a "bound-radical" mechanism. It starts from the bis-(μ-oxo) compound **I** (model of **Q**), forms a weak prereaction complex **II**, and goes over the rate-determining transition state **III** for H-atom abstraction from methane to form a (μ-O)(μ-OH) intermediate **IV** which is weakly complexed with the methyl radical. This intermediate **IV** is presumably short-lived and is not likely to be easily detected experimentally. **IV** goes over a low barrier at transition state **V** for addition of the methyl radical to the μ-OH ligand to give the oxo-methanol complex **VI**. The latter easily eliminates the methanol molecule and produces the Fe(μ-O)Fe, **VII**, complex.

(2) During this process, the oxidation state of the Fe core changes from Fe^{IV}-Fe^{IV} in **I** to a mixed valence Fe^{IV}-Fe^{III} in short-lived intermediate **IV**, and finally to Fe^{III}-Fe^{III} in **VI** and **VII**:

I, $L_4Fe^{IV}(\mu\text{-}O)_2Fe^{IV}L_4 + CH_4 \rightarrow$ **II**, weak prereaction complex

$\rightarrow$ **III**, TS1 for H-atom abstraction (rate-determining)

$\rightarrow$ **IV**, $L_4Fe^{IV}(\mu\text{-}O^2)(\mu\text{-}O^1H(\cdots CH_3))Fe^{III}L_4$ ("bound-radical" intermediate)

$\rightarrow$ **V**, TS2 for CH_3 addition $\rightarrow$ **VI**, $L_4Fe^{III}(O^1HCH_3)(\mu\text{-}O^2)Fe^{III}L_4$

$\rightarrow$ **VII**, $L_4Fe^{III}(\mu\text{-}O_2)Fe^{III}L_4 + (O^1HCH_3)$

Below, in our studies of reactions 1 and 2a, we will follow the same pathway described above. Before describing the mechanisms of these reactions in more detail, we would like first to address the roles of the basis sets and models used in our previous papers once again. To examine the effects of the basis set, we have recalculated the energies of all intermediates and transition states of the reaction of model **I** with the methane molecule at the B3LYP/SBK(+$d_{C,O}$) and B3LYP/SBK(+$d_{C,N,O}$) levels at the B3LYP/SBK optimized geometries and compared with the previous B3LYP/SBK(+$d_{C,O}'$) energies. As seen in Table 1, improvement of the basis set from SBK(+$d_{C,O}'$) through SBK(+$d_{C,O}$) to SBK(+$d_{C,N,O}$) only slightly changes the calculated energetics; the value of the rate-determining H-atom abstraction barrier lies in the range of ca. 22−23 kcal/mol, while the C−O bond formation barrier at TS2 lies in the range of 3−4 kcal/mol. The methyl and methanol dissociation energies calculated from the corresponding complex, **IV** (^{11}A) and **VI** (^{11}A), respectively, change within 4.2−2.6 and 7.2−4.6 kcal/mol. The observed energetic changes are larger upon going from SBK(+$d_{C,O}'$) to SBK(+$d_{C,O}$) than from SBK(+$d_{C,O}$) to SBK(+$d_{C,N,O}$). Therefore, in the discussions of activation of other molecules in the following sections, we will use only the SBK(+$d_{C,O}$) basis set for energy calculations.

To elucidate the effect of the "small" model **I** used in our previous papers, here we have reoptimized the geometries and recalculated the energetics of all intermediates and transition states for the reaction of **Q** with CH_4 using the **I_m** complex (Figure 1) as the "medium" model of compound **Q**. The obtained energies of all intermediates and transition states of the reaction **I_m** with CH_4 are presented in Table 1 and Figure S1 of the Supporting Information, while their reoptimized geometries are given in Figure 2. As seen in Table 1, improving the model system by going from "small", **I**, to "medium", **I_m**, significantly changes the calculated energetics; it reduces the calculated rate-determining H-atom abstraction barrier from 22.8 to 13.3 kcal/mol, which is in excellent agreement with the experimental values, 14−17 (free energy of activation) and 8 (enthalpy of

(31) (a) Musaev, D. G.; Morokuma, K. *J. Phys. Chem.* **1996**, *100*, 6509. (b) Erikson, L. A.; Pettersson, L. G. M.; Siegbahn, P. E. M.; Wahlgren, U. *J. Chem. Phys.* **1995**, *102*, 872. (c) Ricca, A.; Bauschlicher, C. W., Jr. *J. Phys. Chem.* **1994**, *98*, 12899. (d) Heinemann, C.; Hertwig, R. H.; Wesendrup, R.; Koch, W.; Schwarz, H. *J. Am. Chem. Soc.* **1995**, *117*, 495. (e) Hertwig, R. H.; Hrusak, J.; Schroder, D.; Koch, W.; Schwarz, H. *Chem. Phys. Lett.* **1995**, *236*, 194. (f) Schroder, D.; Hrusak, J.; Hertwig, R. H.; Koch, W.; Schwerdtfeger, P.; Schwarz, H. *Organometallics* **1995**, *14*, 312. (g) Fiedler, A.; Schroder, D.; Shaik, S.; Schwarz, H. *J. Am. Chem. Soc.* **1994**, *116*, 10734. (h) Fan, L.; Ziegler, T. *J. Chem. Phys.* **1991**, *95*, 7401. (i) Berces, A.; Ziegler, T.; Fan, L. *J. Phys. Chem.* **1994**, *98*, 1584. (j) Lyne, P. D.; Mingos, D. M. P.; Ziegler, T.; Downs, A. J. *Inorg. Chem.* **1993**, *32*, 4785. (k) Li, J.; Schreckenbach, G.; Ziegler, T. *J. Am. Chem. Soc.* **1995**, *117*, 486.

(32) Frisch, M. J.; Trucks, G. W.; Schlegel, H. B.; Scuseria, G. E.; Robb, M. A.; Cheeseman, J. R.; Zakrzewski, V. G.; Montgomery, J. A., Jr.; Stratmann, R. E.; Burant, J. C.; Dapprich, S.; Millam, J. M.; Daniels, A. D.; Kudin, K. N.; Strain, M. C.; Farkas, O.; Tomasi, J.; Barone, V.; Cossi, M.; Cammi, R.; Mennucci, B.; Pomelli, C.; Adamo, C.; Clifford, S.; Ochterski, J.; Petersson, G. A.; Ayala, P. Y.; Cui, Q.; Morokuma, K.; Malick, D. K.; Rabuck, A. D.; Raghavachari, K.; Foresman, J. B.; Cioslowski, J.; Ortiz, J. V.; Stefanov, B. B.; Liu, G.; Liashenko, A.; Piskorz, P.; Komaromi, I.; Gomperts, R.; Martin, R. L.; Fox, D. J.; Keith, T.; Al-Laham, M. A.; Peng, C. Y.; Nanayakkara, A.; Gonzalez, C.; Challacombe, M.; Gill, P. M. W.; Johnson, B. G.; Chen, W.; Wong, M. W.; Andres, J. L.; Head-Gordon, M.; Replogle, E. S.; Pople, J. A. *Gaussian 98*, revision A.7; Gaussian, Inc.: Pittsburgh, PA, 1998.

Table 1. Total (in Italic, in hartree) and Relative (in kcal/mol, Relative to the ^{9}A Reactants) Energies of Various Intermediates and Transition States in the ^{9}A and ^{11}A States for the Reaction of "Medium", **I_m**, and "Small", **I**, Models with CH_4, Calculated with Different Basis Sets at the Optimized Geometries with the SBK Basis Set[a]

		small model			medium model
structures basis set		SBK(+$d_{C,O}'$)[b]	SBK(+$d_{C,O}$)[c]	SBK(+$d_{C,N,O}$)	SBK(+$d_{C,N,O}$)
		^{9}A-state			
reactants	**I** + CH_4	0.0	0.0	0.0	0.0
		−419.775345	*−419.799347*	*−419.813096*	*−518.012089*
CH_4 complex	**II**	−1.5	−1.0	−1.2	−0.7
TS1 (C−H)	**III**	23.2	21.8	22.8	13.3
OH···CH_3 complex	**IV**	11.3	9.5	10.6	1.7
TS2 (O−CH_3)	**V**	20.6	19.0	18.5	8.4
CH_3OH complex	**VI**	−41.8	−43.7	−42.9	−48.4
CH_3OH dissociation	**VII**	−34.3	−39.0	−38.1	−42.1
CH_3 dissociation	**VIII**	15.5[d]	11.1	13.3	3.4
		^{11}A-state			
reactants	**I** + CH_4	5.4/0.0	3.7/0.0	4.8/0.0	5.6/0.0
		−419.766739	*−419.793418*	*−419.805528*	*−518.003234*
CH_4 complex	**II**	4.2/−1.2	2.7/−1.0	3.8/−1.0	4.7/−0.9
TS1 (C−H)	**III**	24.4/19.0	22.2/18.5	23.2/18.4	17.1/11.5
OH···CH_3 complex	**IV**	11.3/5.9	9.4/5.7	10.7/5.9	2.3/−3.3
TS2 (O−CH_3),	**V**	18.6/13.2	18.8/15.1	22.7/17.9	9.6/4.0
CH_3OH complex	**VI**	−53.9/−59.3	−54.1/−57.8	−52.8/−57.6	−61.9/−67.5
CH_3OH dissociation	**VII**	−46.7/−52.1	−49.5/−53.2	−48.2/−53.0	−50.2/−55.8
CH_3 dissociation	**VIII**	15.5/10.1	11.1/7.4	13.3/7.5	3.4/−2.2

[a] The numbers after slash are relative to the ^{11}A reactants. [b] These results are taken from our previous paper, where d-functions were included only on the O-atoms of O_2-fragment and C-atom of the methane molecule. [c] These results were obtained by including d-functions to all C and O atoms. [d] Previously, this number was reported to be 23.7 kcal/mol, which corresponded to the excited ^{8}A state of **VIII** lying 8.2 kcal/mol higher than the ground ^{10}A state.

activation) kcal/mol, reported by Lippard and co-workers.[2,33] It only slightly (by 1.2 kcal/mol) reduces the C−O bond formation barrier at TS2, which is found to be only 7−8 kcal/mol. The "bound-radical" complex **IV** is stabilized by 8−9 kcal/mol, while the methyl dissociation energy calculated from this complex is reduced only slightly to 1.7 (^{9}A) and 1.1 (^{11}A) kcal/mol. The increased methanol dissociation energy from 4.6 to 11.7 kcal/mol for ^{11}A state is more noticeable.

These large changes in the calculated energies upon going from model **I** to **I_m** could be a result of several factors. The first factor is the change in the electronic properties of the bridging O^1-center, directly involved in the reaction, due to the change in ligand environment of the Fe-centers. Indeed, in the "small" model, **I**, the O^1-center is located trans to the strong NH_2^- ligands which forms strong Fe−NH_2 covalent bonds, while in the "medium" model, **I_m**, the ligands located trans to the O^1-center are imidazoles, which form relatively weak donor−acceptor bonds with the Fe-centers. Ligands located cis to the O^1-center in model **I** are water ligands which form relatively weak bonds with Fe-centers, while the carboxylate ligands of model **I_m** located cis to the O^1-center form stronger bonds with Fe-centers. The calculated atomic spin densities, presented in Table 2, support the above-presented discussion. Indeed, the spin density (e.g., electronic properties) of the bridging O^1-center directly involved in the reaction changes significantly upon going from model **I** to model **I_m**, especially for the ^{11}A states. As seen in Table 2, in the "small" model, **I**, the O^1-center (from where the O-side pathway starts) has spin densities of 0.30 e and 0.43 e, while the O^2-center, which was found[17] to be more reactive (N-side mechanism), has relatively large, 0.44 e and 1.03 e, spin densities for the ^{9}A and ^{11}A states, respectively. In the model **I_m**, it is the O^1-center that has large, 0.30 e and 1.17 e, spin densities, for the ^{9}A and ^{11}A states, respectively, and the calculated spin densities on the O^2-center are 0.24 e and 0.38 e for the ^{9}A and ^{11}A states, respectively. In other words, it could be expected that upon going from model **I** to model **I_m**, the O^1-center (O-side mechanism) will become more reactive than the O^2-center (N-side mechanism).[17,18] That is an another reason why below we study only the O-side mechanism of the reaction **Q** + substrate.

The second reason of why the calculated energetics of the **Q** + CH_4 reaction were significantly different between model **I** and model **I_m** could be the existence of several additional hydrogen bonding (H-bonding) interactions in the intermediate and transition state structures in the **I_m** model. Indeed, as seen in Figure 2, where we have presented the calculated intermediates and transition states and their geometrical parameters, the "open leg" of the terminal carboxylate ligands tends to form weak H-bonds in structures **IV**, **VI**, and **VIII**. In structure **VII** one of the terminal carboxylates moved to a bridging position between two Fe-centers. All these additional structural changes, found in the "medium" model studies, were not seen in the "small" model studies reported previously.[17,18]

Concluding this section, improving the basis set from SBK(+$d_{C,O}'$) to SBK(+$d_{C,O}$) and SBK(+$d_{C,N,O}$) does not significantly change the calculated energetics. The observed changes are larger upon going from SBK(+$d_{C,O}'$) to SBK(+$d_{C,O}$) than from SBK(+$d_{C,O}$) to SBK(+$d_{C,N,O}$). Therefore, below we will use only the SBK(+$d_{C,O}$) basis set for energy calculations. The use of the "medium" model, **I_m**, in these studies also did not change our qualitative conclusions made on the basis of "small" model, **I**, studies, while it significantly changed the calculated energetics. These studies once again demonstrated the usefulness of our "small" model, which provides qualitatively the same results as "medium" or "large" models, neither of which takes into account protein environment beyond the first shell. Therefore, below we will use only the "small" model for compound **Q** in our studies. We are aware that the calculated

(33) Liu, K. E.; Valentine, A. M.; Wang, D.; Huynh, B. H.; Edmondson, D. E.; Salifoglou, A.; Lippard, S. J. *J. Am. Chem. Soc.* **1995**, *117*, 10174.

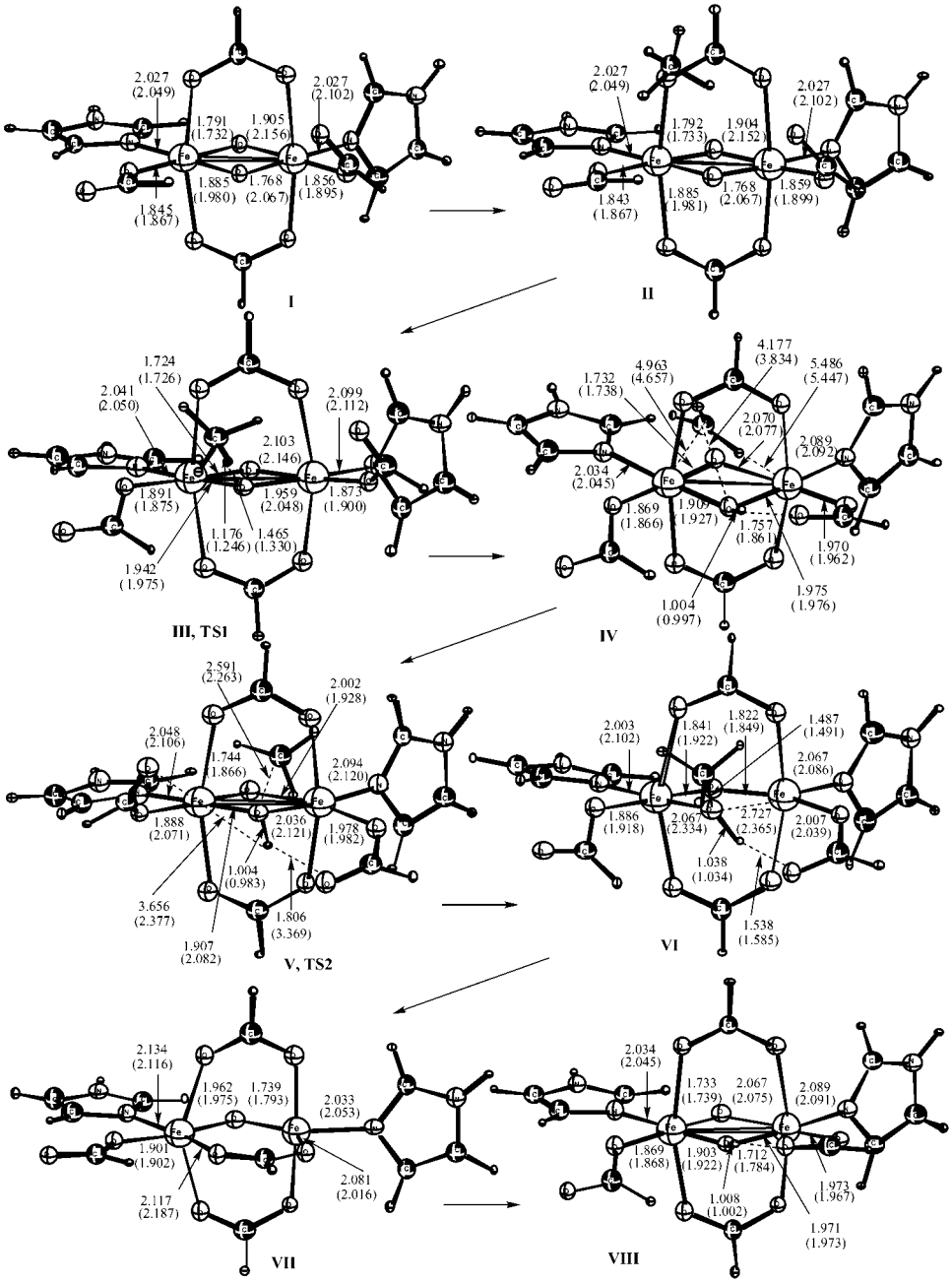

Figure 2. The calculated important bond distances (in Å) of the intermediates and transition states of the reaction of complex **I_m** with methane for both the ^{9}A and the ^{11}A (in parentheses) states.

energetics for these "small" model studies could be significantly (up to 9−10 kcal/mol) different from their most realistic value, but the correctness of the qualitative conclusions based on the relative changes in the barrier heights between different substrates is without doubts. Thus, below, throughout of this paper, we use "small" model, **I**, for compound **Q**, with the B3LYP/SBK method for geometry optimization and the B3LYP/SBK(+$d_{C,O}$)//B3LYP/SBK method for the energetics.

B. Effects of Substrate Molecules. Reaction of I with C_2H_6 and CH_3F, and Comparison with CH_4. Below, we report our results on the mechanism of the reaction of compound **Q** with the ethane and methyl fluoride molecules proceeding via the O-atom insertion into the C−H bond, reaction 1. We follow the same reaction path reported[17,18] for the reaction of **I** with substrate CH_4. It starts with the asymptotic **I** + substrate, forms the prereaction complex **II**, goes through the H-atom abstraction transition state **III** (TS1) leading to the bond-radical complex **IV**, followed by the C−O bond formation transition state **V** (TS2) to form the product complex **VI**. We believe that the comparison of results for ethane and methyl fluoride with those for the methane molecule[18] will allow us to elucidate the effects of the X-group of XCH_3 in the hydrocarbon hydroxylation reaction catalyzed by compound **Q**, where X = H (for methane), F (for methyl fluoride), and CH_3 (ethane). In Table 3, as well as Figure 3, we present all the calculated energetics of the reaction of **I** with CH_4 (for comparison), CH_3F, C_2H_6, and compare them with each other. In Figures 4 and 5 we present the structures and geometries of the calculated intermediates and transition states for substrates C_2H_6 and CH_3F, respectively; those for CH_4 were reported in our previous paper.[18]

Table 2. Mulliken Atomic Spin Densities (in e) for the Various Intermediates and Transition States of Reaction of "Medium" (before Slash), **I_m**, and "Small" (after Slash), **I**, Models with Methane, Calculated at the B3LYP/SBK Level[a]

	atomic spin densities (in e)					
structures	L_nFe^2	L_nFe^1	O^2	O^1	H^b	$CH_3{}^c$
			^{9}A-state			
I	3.57/3.55	3.52/3.44	0.24/0.44	0.30/0.30		
II	3.57/3.52	3.52/3.43	0.24/0.44	0.30/0.31		
III	3.46/3.54	4.45/3.59	0.40/0.40	−0.40/−0.37	0.02/0.06	−0.32/−0.55
IV	3.43/3.51	4.46/4.64	0.43/0.43	0.26/0.08	0.01/0.00	−1.17/−0.99
V	3.31/3.23	4.45/4.58	0.33/0.38	0.30/0.20	0.00/0.00	−0.93/−0.73
VI	2.87/2.92	4.31/4.54	0.42/0.35	0.03/0.00	0.00/0.00	0.00/0.00
VII	2.76/2.95	4.56/4.52	0.40/0.38			
VIII[d]	−/1.69	−/4.52	−/0.56	−/0.07	−/0.00	
			^{11}A-state			
I	3.33/3.47	4.48/4.62	0.38/1.03	1.17/0.43		
II	3.33/3.47	4.48/4.62	0.39/1.03	1.17/0.43		
III	3.39/3.52	4.50/4.63	0.42/0.43	0.78/0.55	−0.02/-0.07	0.50/0.59
IV	3.43/3.58	4.57/4.67	0.42/0.43	0.25/0.10	0.00/0.00	1.17/0.98
V	3.67/3.97	4.70/4.57	0.44/0.50	0.17/0.01	0.01/0.01	0.98/0.81
VI	4.34/4.59	4.32/4.48	0.71/0.66	0.07/0.00	0.00/0.00	0.00/0.00
VII	4.37/4.54	4.25/4.54	0.75/0.67			
VIII	3.42/4.54	4.57/4.65	0.42/0.42	0.26/0.08	0.00/0.00	

[a] Here, L_nFe stands for the (HCOO)(Imd)Fe-fragment. This table does not include the portion of spin densities located on the bridging carboxylate ligands, each of which may have about 0.10−0.25 e spin. [b] H atom located between O^1 and CH_3 fragments. [c] The number for the entire CH_3 fragment. [d] For the complex **VIII** we have calculated ^{8}A (only at the "small" model studies) and ^{10}A spin states.

Table 3. Total (in Italic, in hartree) and Relative (in kcal/mol, Relative to the ^{9}A Reactants) Energies of Various Intermediates and Transition States, for ^{9}A and ^{11}A States, for the Reaction of Complex **I** with Methane, Methyl Fluoride, and Ethane, Calculated at the B3LYP/SBK(+$d_{C,O}$)//B3LYP/SBK Level[a]

structure		CH_4	FCH_3	C_2H_6
		^{9}A-state		
reactants	XCH_3 + **I**	0.0	0.0	0.0
		−419.799347	*−443.373829*	*−426.651169*
XCH_3 complex	**II**	−1.0	−4.1	0.2
TS1 (C−H activation)	**III**	21.8	18.8	18.5
OH···CH_2X complex	**IV**	9.5	4.2	5.1
TS2 (O−CH_2X formation)	**V**	19.0		
CH_2XOH complex	**VI**	−43.7	−52.2	−50.5
CH_2XOH dissociation	**VII**	−39.0	−49.9	−42.1
CH_2X dissociation	**VIII**	11.1	7.6	7.1
		^{11}A-state		
reactants	XCH_3 + **I**	3.7/0.0	3.7/0.0	3.7/0.0
		−419.793418	*−443.367900*	*−426.645240*
XCH_3 complex	**II**	2.7/−1.0	2.3/−1.4	4.0/0.3
TS1 (C−H activation)	**III**	22.2/18.5	22.3/18.6	22.7/19.0
OH···CH_2X complex	**IV**	9.4/5.7	7.4/3.7	2.5/−1.2
TS2 (O−CH_2X formation)	**V**	18.8/15.1		
CH_2XOH complex	**VI**	−54.1/−57.8	−68.3/−72.0	−65.5/−69.2
CH_2XOH dissociation	**VII**	−49.5/−53.2	−60.4/−64.1	−52.6/−56.3
CH_2X dissociation	**VIII**	11.1/7.4	7.6/3.9	7.1/3.4

[a] The numbers after slash are relative to the ^{11}A reactants.

Because the electronic and geometrical structures of complex **I** have been discussed in our previous paper,[17] here we will not repeat those discussions. Here, once again, we would like to point out that of the calculated ^{9}A and ^{11}A states, the ^{9}A state is lower in energy by 3.7 kcal/mol at the B3LYP/SBK(+$d_{C,O}$)// B3LYP/SBK level used throughout the present paper.

As was mentioned above, the reaction of **I** with the hydrocarbons starts with coordination of the hydrocarbon to **I** to form the prereaction complex, **II**. This process is found to be exothermic by 1.0(1.0) and 4.1(1.4) kcal/mol for methane and methyl fluoride, respectively, while it is slightly, 0.2(0.3) kcal/mol, endothermic for ethane. Note that throughout this paper the numbers given without parentheses correspond to the ^{9}A state, while those in parentheses to the ^{11}A state. These differences in the reaction energies could be explained in terms of larger steric repulsion between C_2H_6 and the rest of the complex, as compared with CH_4 and CH_3F. The 3 kcal/mol difference in the stabilization energies of methane and methyl fluoride complexation could be the result of several factors including the following: (1) The existence of an H-bonding interaction between terminal water and F atom. The calculated HOH···FCH_3 distance is 1.689(1.719) Å. This HOH···FCH_3 interaction is ubiquitously present in all the calculated FCH_3 substrate complexes and transition states. (2) The existence of the stronger interaction between the negatively charged (−0.22 e) O^1-center and H^b-atom of FCH_3 than in the CH_4 complex because of the difference in the electronegativity of the F and H atoms and in the C−H^b bond energies of these substrates. Indeed, as it was expected, the replacement of the terminal H with F redistributes the electron density in the substrate and makes the bridging H^b-atom relatively more positively charged in FCH_3, +0.19 e, than in HCH_3, +0.17 e. (3) Difference in

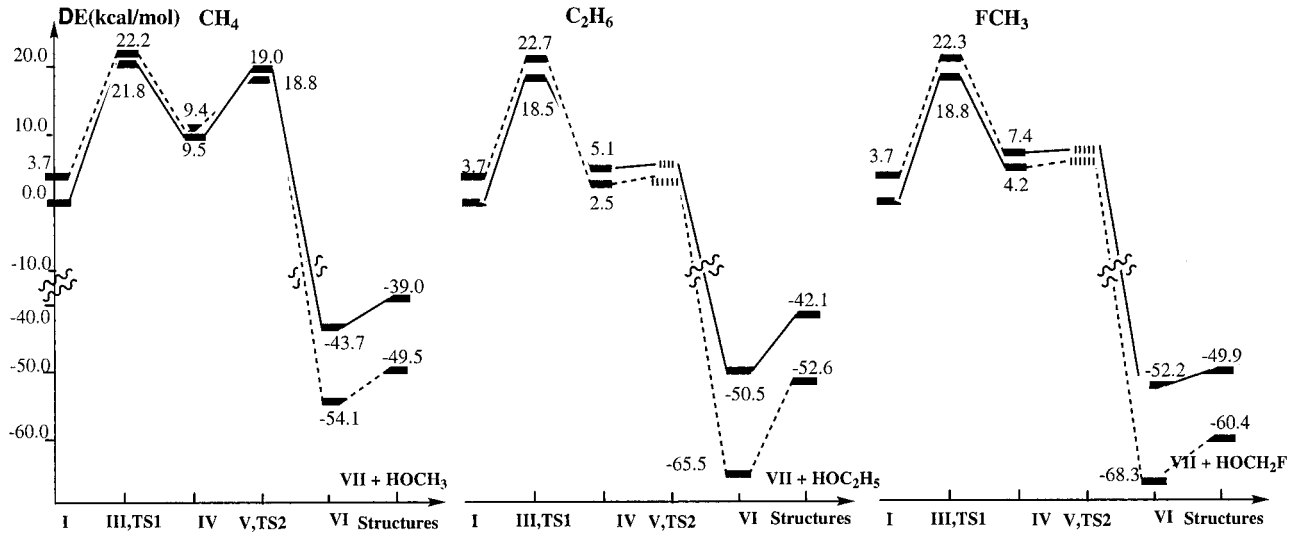

Figure 3. Schematic representation of the potential energy profile (in kcal/mol) of ^{9}A (solid line) and ^{11}A (dashed line) states of reaction of complex **I** with methane, ethane, and methyl fluoride calculated at the B3LYP/SBK(+$d_{C,O}$)//B3LYP/SBK level. Note that TS2s for the reaction of **I** with ethane and methyl fluoride molecules were not studied.

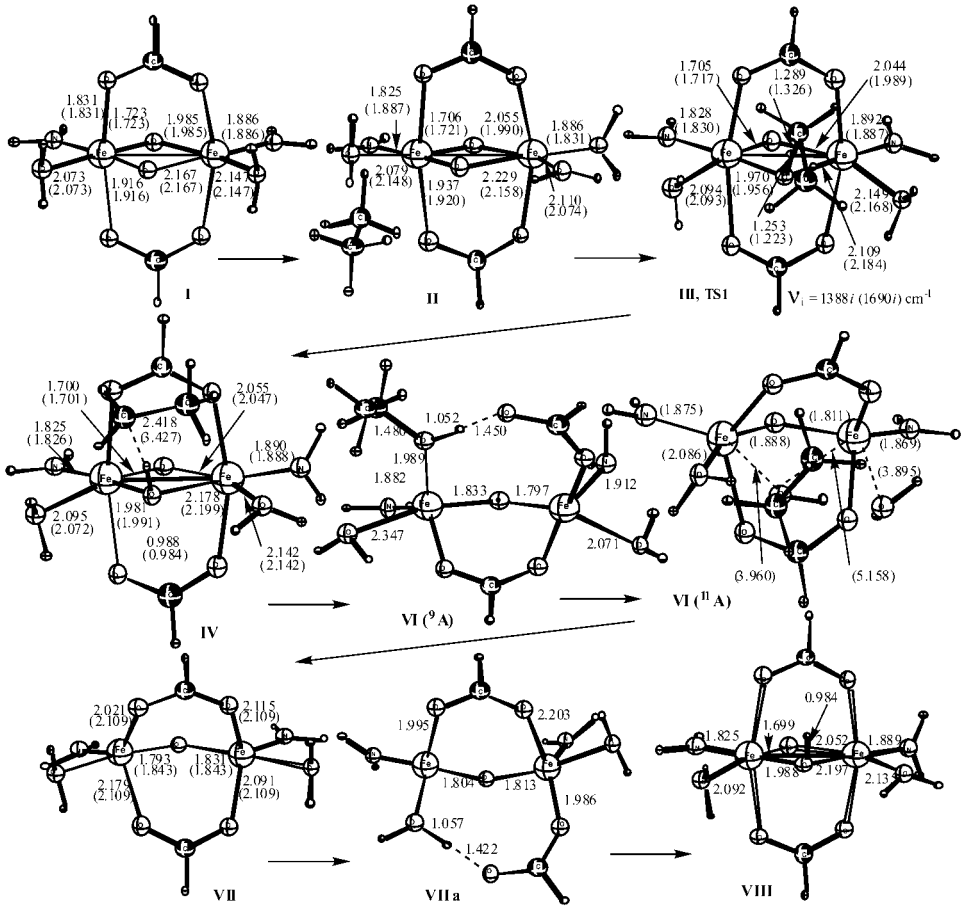

Figure 4. The calculated important bond distances (in Å) of the intermediates and transition states of the reaction of complex **I** with ethane for both the ^{9}A and the ^{11}A (in parentheses) states.

the C−H^b bond energies,[34] which are 104.8 ± 0.2 kcal/mol in the CH_4 and 101.2 ± 1 kcal/mol in FCH_3. As a result of the factors (2) and (3), the H^b interacts stronger with a negatively charged O^1 center in FCH_3 than in HCH_3. Indeed, as seen in Figure 5, the calculated O^1- -H^b bond distances are 2.179(2.278) Å for FCH_3, while previously it was calculated to be 2.699-(2.896) Å for CH_4.

The next step is the C−H(H^b) bond activation via the H^b-atom abstraction by the bridging O^1-atom at the transition state **III**, TS1. As was previously[18] shown, this is the rate-determining

(34) *CRC Handbook of Chemistry and Physics*, 72nd ed.; Lide, D. R., Ed.; CRC Press: Boca Raton-Ann Arbor-Boston, 1991−1992.

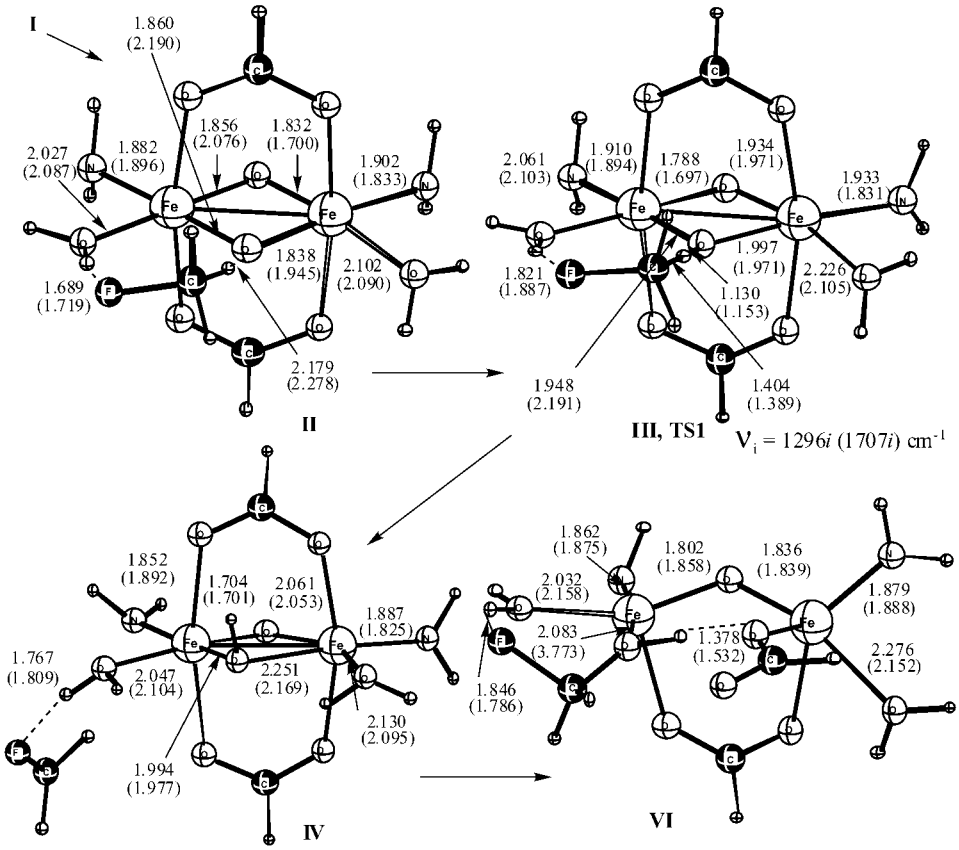

Figure 5. The calculated important bond distances (in Å) of the intermediates and transition states of the reaction of complex **I** with methyl fluoride for both the ^{9}A and the ^{11}A (in parentheses) states.

step of the entire methane activation process. As is seen from Table 3 and Figure 3, the H^b-atom abstraction barrier at transition state **III** is a few kcal/mol lower for ethane and methyl fluoride than for the methane substrate; TS1 is calculated to be 18.8(18.6) kcal/mol for CH_3F, 18.5(19.0) kcal/mol for C_2H_6, and 21.8(18.5) kcal/mol for CH_4, from the reactant of the respective spin state. Concerning only the ground ^{9}A-state, the trend in the calculated H^b-abstraction barriers, CH_4 (21.8 kcal/mol) > CH_3F (18.8 kcal/mol) ≥ C_2H_6 (18.5 kcal/mol), is consistent with the C−H^b bond strength in these substrates, which is found to be 104.8 ± 0.2, 101.2 ± 1.0, and 100.3 ± 1.0 kcal/mol for the methane, methyl fluoride, and ethane, respectively.[34] Thus, the weaker the C−H^b bond, the lower is the H^b-abstraction barrier. At first glance, our data for ethane and methane molecules seem to contradict the available experimental findings,[4] indicating that the kinetics for methane are faster than any other alkanes reacting with MMO. However, the recent experimental studies[35] suggest that the rate-determining step of the reaction of **Q** with S depends on many factors including (a) the size of the substrate, (b) C−H bond strength, and (c) protein dynamics. Because our studies take into account only one of these factors, C−H bond strength, our data cannot be directly compared with the available experiments. However, our results allow one to draw the conclusion that the weaker C−H^b bond, the smaller is the H^b-abstraction barrier by compound **Q**.

The calculated geometries of TS1 for ethane are more "reactant-like" than those for methane substrate; as is seen in Figure 4, the calculated O^1−H^b and C−H^b distances are 1.253(1.223) Å and 1.289(1.326) Å for the **I** + ethane reaction, while these values are 1.207(1.203) Å and 1.328(1.344) Å for the methane substrate. This effect could be explained in terms of the reduced positive charge of H^b atom upon going from the methane molecule (+0.17 e) to ethane (+0.13 e), which results in the weaker interaction with the negatively charged O^1-center.

Transition state **III** for the CH_3F substrate is found to be more "product-like"; the calculated O^1−H^b and C−H^b bond distances are 1.130(1.153) and 1.404(1.389) Å, respectively. The "product-like" nature of the TS1 for CH_3F as compared with the ethane and methane nicely fits the above given explanation based on the charge distributions within the substrate molecules. Indeed, the replacement of H atom in CH_4 by F atom makes the H^b-atom more positively charged in CH_3F, +0.19e , as compared with +0.17 e in CH_4, and results in the stronger interaction of the negatively charged O^1-center, −0.22 e.

Thus, the above-presented data clearly show that the replacement of a H-atom in a methane molecule with more electronegative groups (or atoms) tends to increase the positive charge on H^b, and makes the H^b-abstraction transition state less "reactant-like". In contrast, the replacement of the H-atom in CH_4 with less electronegative groups (or atoms) reduces the positive charge on H^b atom and makes the H^b-abstraction transition state more "reactant-like".

The frequency calculation for structures **III** confirms that they are real transition states with one imaginary frequency of 1388*i*(1690*i*) cm^{-1} and 1286*i*(1707*i*) cm^{-1} for ethane and methyl fluoride, respectively. The main components in this imaginary

(35) Brazeau, B. J.; Wallar, B. J.; Lipscomb, J. D. *J. Am. Chem. Soc.* **2001**, *123*, 10421.

frequency mode are the forming O^1-H^b and broken $C-H^b$ stretches corresponding to the H^b-atom abstraction process.

Overcoming TS1 leads to the formation of the bound-radical complex, **IV**. The ground electronic state of this complex is found to be ^{11}A state for the ethane substrate, while it is a ^{9}A state for methyl fluoride and methane substrates. In any case, the calculated ^{9}A and ^{11}A states of **IV** are energetically very close to each other. This suggests that these two electronic states, ^{9}A and ^{11}A, cross each other in the vicinity of **IV**. The calculated Mulliken spin densities indicate that Fe-centers of the complex **IV** are a five-spin Fe^1(III) with spin densities of 4.5−4.6 e directly on Fe (with the rest delocalized), and a four-spin Fe^2-(IV) with spin densities of 3.2−3.3 e directly on Fe. The alkyl radical has almost one unpaired spin parallel and antiparallel to the spins of the Fe-centers in the case of the ^{11}A state and the ^{9}A state, respectively. The process **I** + substrate → **IV** is relatively less endothermic for ethane and methyl fluoride than for methane substrate. The calculated (ca. 4−5 kcal/mol) difference in the relative stability (relative to the corresponding reactants) of the corresponding biradical complexes **IV** for ethane, methyl fluoride, and methane, most likely, is a result of the lack of the H-bonding interaction in the latter. The calculated $C-H^b$ distance in bound-radical complex **IV** is 2.418-(3.427) Å for ethane, and 2.484(2.561) Å for methane substrates. On the other hand, for CH_3F as shown in Figure 5, the FCH_2 radical is effectively dissociated and held by the $HOH\cdots FCH_3$ H-bond.

As was shown previously,[17,18] the next step of reaction should be $C-O^1$ bond formation between the carbon atom of the alkyl radial and the O^1 atom of the O^1H-bridge. Unfortunately, we were not able to locate the transition state (TS2) corresponding to this process for the ethane and methyl fluoride substrates. All our efforts to find TS2 for ethane substrate led to either the formation of ethanol complex **VI** or the transition state for H-atom transfer from C_2H_5 to O^1H to give water and an ethylene complex. Similarly, Siegbahn and co-workers[24f] could not find TS2 for the same reaction and explained that the radical rebinding step becomes a cation rebinding step (after H-abstraction) due to electron transfer from the incipient radical to the Fe-centers. In the case of CH_3F, all our attempts to locate the C−O bond formation transition state led to either complex **IV** or complex **VI**. Because we have shown previously[17,18] for the methane substrate that the alcohol formation process is not the rate-determining step of hydrocarbon hydroxylation catalyzed by complex **I**, here we did not further pursue the search for TS2 for ethane and methyl fluoride substrates. We expect that the transition state TS2 is geometrically very close to intermediate **IV** with a small barrier of only a few kcal/mol.

The ground state of the resultant alcohol complex **VI** is found to be the ^{11}A state, which lies 50.5(65.5) kcal/mol and 52.2-(68.3) kcal/mol lower than that of the reactants for C_2H_6 and FCH_3, respectively. As seen in Figure 4, there are distinct structural differences for the ^{11}A and ^{9}A states of complex **VI** for the ethane substrate. In the ^{11}A state, the formed ethanol molecule is almost dissociated from the complex, with the Fe−O(H)(C_2H_5) distances of (3.960) and (5.158) Å. Also, one of the terminal water molecules (on Fe^1) is almost dissociated with the Fe^1-OH_2 distance of (3.895) Å. On the other hand, in the ^{9}A state, the ethanol molecule is relatively strongly coordinated to the Fe^2-center with the $Fe^2-O(HOC_2H_5)$ bond distance of 1.989 Å, and one of the "legs" of the bridged carboxylate is opened with a strong H-bond formed with the ethanol molecule with the $OC(H)O\cdots HO$ C_2H_5 distance of 1.450 Å.

Geometries of the $HOCH_2F$-complex, structure **VI** in Figure 5, also show distinct differences between the ^{9}A and ^{11}A states. In the ^{9}A state FCH_2OH is attached to the Fe^2-center, and H-bonded to one of the terminal (on Fe^1) carboxylates with the FCH_2-OH bond distance of 2.083 Å. In the ^{11}A state FCH_2-OH is only H-bonded to rest of the molecule, with the Fe−$OHCH_2F$ distance of (3.773) Å, and it effectively is located in the outer sphere.

In the last step of the reaction the alcohol molecule dissociates from complex **VI** to give complex **VII**. The process **VI** → **VII** + alcohol is calculated to be endothermic by 7.5(7.2), 8.4(12.9), and 2.3(7.9) kcal/mol for the $HOCH_3$, HOC_2H_5, and $HOCH_2F$, respectively. Because we have discussed complex **VII** in our previous paper,[17,18] we will not discuss it in more details again. Here, we only would like to point out that the ground state of complex **VII** is an Fe^{III}-Fe^{III} complex with two high-spin Fe's in the ^{11}A state, while one Fe^1 is a high-spin Fe^{III}, and Fe^2 is a low-spin Fe^{III} in the ^{9}A state. Because the intraatomic spin coupling in the Fe^{III} center is energetically costly, the ^{9}A state of complex **VII** lies energetically higher than the ^{9}A state.

We also have calculated the alkyl radical dissociation from the bound radical complex **IV** leading to complex **VIII** and alkyl radical. Because complex **IV** is Fe^{III}-Fe^{IV} complex with two high-spin iron atoms for both ^{9}A and ^{11}A states, for the product complex **VIII** we have calculated only the ^{10}A state corresponding to Fe^{III}-Fe^{IV}. The results presented in Table 3 show that the process **IV** (ground state: ^{9}A for CH_4 and CH_3F, ^{11}A for C_2H_6) → **VIII** (^{10}A) + R (doublet) is endothermic by 1.7, 3.8, and (4.6) kcal/mol for R = CH_3, CH_2F, and C_2H_5, respectively. The few kcal/mol difference in the radical dissociation energies could be explained in terms of the existence of H-bonded interactions in the CH_2F and C_2H_5 complexes, which is lacking for CH_3 (see Figures 4 and 5). One should note that reaction **I** (^{9}A) + RH → **VIII** (^{10}A) + R (doublet) is calculated to be endothermic, and its endothermicity increases via RH = C_2H_6 (7.1 kcal/mol) < CH_3F (8.0 kcal/mol) < CH_4 (11.1 kcal/mol). This trend is a direct reflection of the strength of the C−H bond, C_2H_6 (100.3 ± 1.0 kcal/mol) < CH_3F (101.2 ± 1.0 kcal/mol) < CH_4 (104.8 ± 0.2 kcal/mol);[34] that is, the stronger the C−H bond, the more endothermic is the process.

C. Reaction of Model I with Ethylene. Keeping the above-presented discussions in mind, let us discuss the mechanism of the reaction of **I** (model of complex **Q**) with the ethylene molecule. In general, this reaction may proceed by two distinct pathways: either via the insertion of the bridged O^1 atom into a C−H bond to give the HOC_2H_3 product (reaction 2a, below it will be called the C−H bond insertion pathway), or via the epoxidation (with the oxygen atom bridging the olefinic carbon atoms) pathway leading to the ethylene oxide OC_2H_4 product (reaction 2b, below it will be called the epoxidation pathway). The calculated intermediates and transition states of these two reactions, 2a and 2b, are presented in Figures 6 and 7, respectively, while their energies are given in Table 4 and Figure 8.

For reaction of model **I** with the ethylene molecule we located the prereaction complex **II**, the formation of which is exothermic by 5.2(4.7) kcal/mol. As expected for a substrate with a double

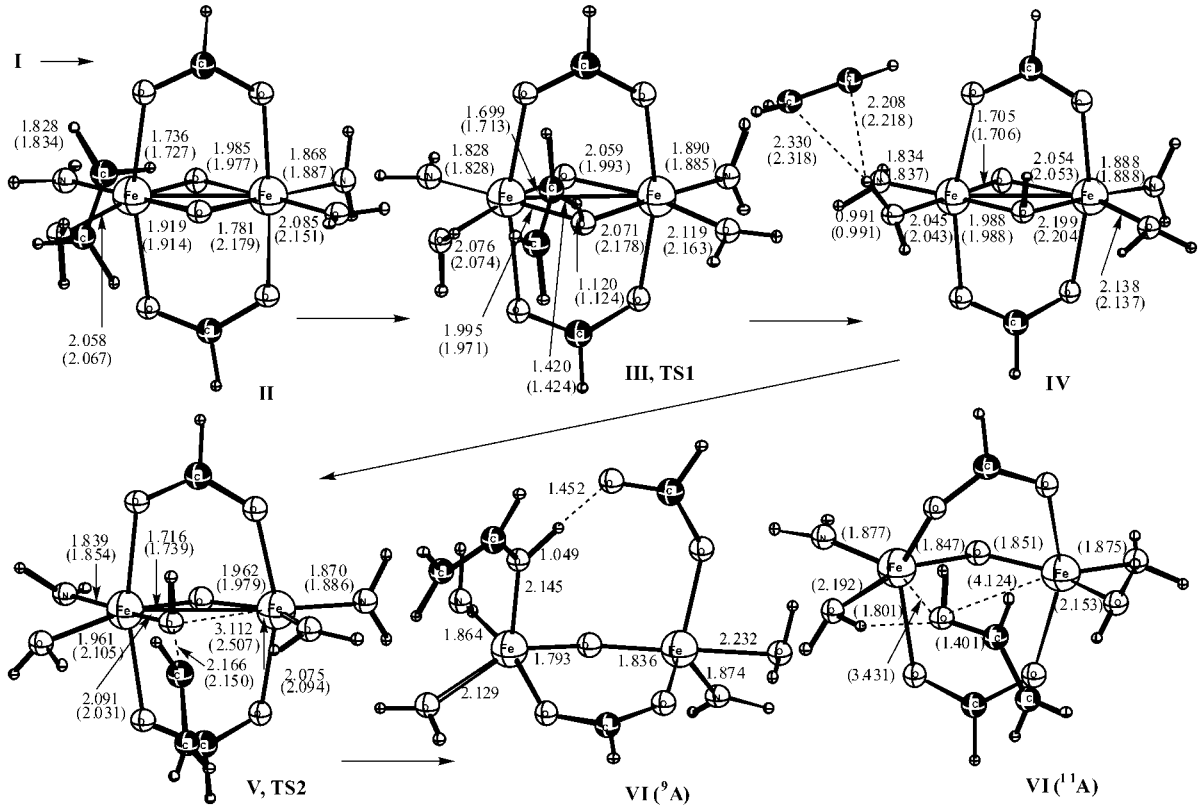

Figure 6. The calculated important bond distances (in Å) of the intermediates and transition states of the reaction of complex **I** with ethylene via C−H bond insertion mechanism for both the ^{9}A and the ^{11}A (in parentheses) states.

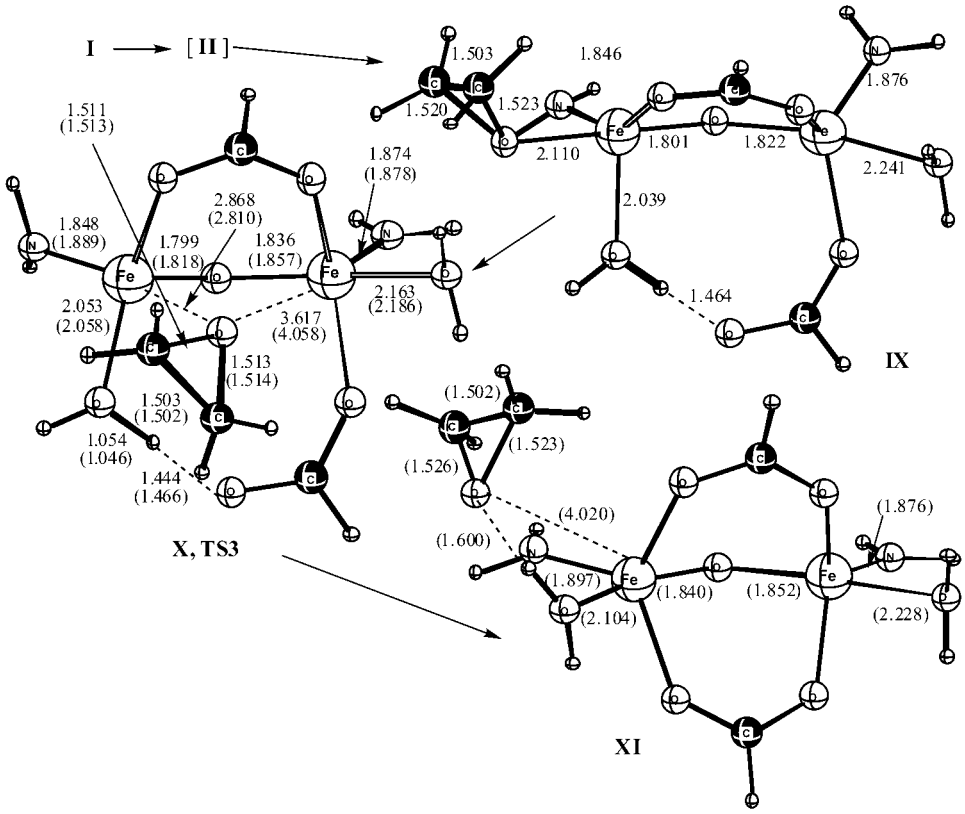

Figure 7. The calculated important bond distances (in Å) of the intermediates and transition states of the reaction of complex **I** with ethylene via epoxidation mechanism for both the ^{9}A and the ^{11}A (in parentheses) states.

bond, the stability of this prereaction complex is larger than that for the aliphatic substrates studied in the preceding sections. Because the weakly bonded complex **II** is not likely to make a significant contribution to the reaction mechanisms, below we

Table 4. Total (in Italic, in hartree) and Relative (in kcal/mol, Relative to the ^{9}A Reactants) Energies of Various Intermediates and Transition States, for ^{9}A and ^{11}A States, for the Reaction of Complex **I** with Molecule of Ethylene, Calculated at the B3LYP/SBK(+$d_{C,O}$) Level[a]

structure		^{9}A-state	^{11}A-state
	insertion into C−H bond		
reactants	C_2H_4 + **I**	0.0 (*−425.406704)*	3.7/0.0 (*−425.400775)*
C_2H_4 complex	**II**	−5.2	−1.7/−4.7
TS1 (C−H activation)	**III**	20.1	23.3/19.6
hydroxy vinyl complex	**IV**	10.4	10.6/6.9
TS2 (O−$CHCH_2$ formation)	**V**	21.9	19.6/15.9
C_2H_3OH complex	**VI**	−53.7	−61.9/−65.6
C_2H_3OH dissociation	**VII**	−50.6	−61.0/−64.7
C_2H_3 dissociation from **IV**	**VIII**	16.7	16.7/13.0
	epoxidation		
C_2H_4O complex	**IX**	−44.7	−62.7
TS (C_2H_4O dissociation)	**X**	−29.8	−54.6
C_2H_4O dissociation	**XI**	−39.3	−53.5

[a] The numbers after slash are relative to the ^{11}A reactants.

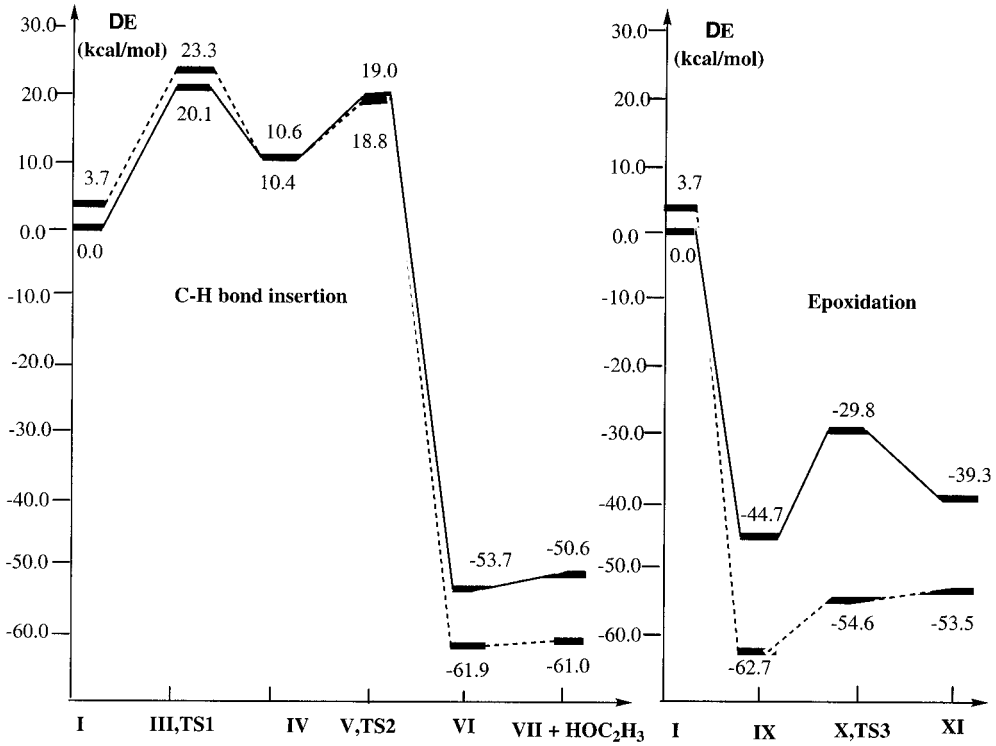

Figure 8. The potential energy profiles (in kcal/mol) of the reaction of complex **I** with ethylene via C−H bond insertion and epoxidation pathways for both the ^{9}A (solid line) and the ^{11}A (dashed line) states.

will not discuss it in more detail, and we will start our discussions from the reactants, complex **I** and the ethylene molecule.

First, let us discuss the C−H bond insertion pathway. This pathway includes the intermediates and transition states similar to those of the above-studied reactions for CH_4, CH_3F, and C_2H_6. From complex **II** (or from the reactants) the reaction proceeds via TS1, **III**, corresponding to the H^b-atom abstraction process, as shown in Figure 6. As shown above, the increase in the positive charge on H^b atom increases the H^b−O^1 interaction, and makes the H^b-abstraction transition state more "product-like". Because H^b is slightly more positively charged in C_2H_4, +0.18 e, than in CH_4, +0.17 e, one expects that TS1 for C_2H_4 is more "product-like". The calculated O^1−H^b and C−H^b bond distances are 1.120(1.124) and 1.420(1.424) Å for ethylene, and 1.207(1.203) and 1.328(1.344) Å for methane, respectively, indicating that TS1 is more "product-like" for ethylene than for methane. The calculated barrier for C_2H_4, 20.1(19.6) kcal/mol, is slightly smaller than 21.8(18.6) kcal/mol for CH_4, despite that the C−H bond strength is slightly larger in C_2H_4, 106 kcal/mol,[34] than in CH_4, 104.8 ± 0.2 kcal/mol.[34] The structure of the transition state **III** in Figure 6 suggests that the π-orbitals of ethylene are interacting with a metal center, providing extra stabilization to lower the barrier.

Overcoming the transition state **III** leads to the hydroxy vinyl complex **IV**, formally written as $L_4Fe(\mu\text{-}O)(\mu\text{-}OH)(C_2H_3)FeL_4$, with the vinyl radical weakly interacting via a $OH\cdot\cdot C_2H_3$ interaction (see Figure 6). The geometries for the ^{9}A and ^{11}A states are very close to each other, indicating a weak interaction between the vinyl radical and complex **VIII**. Indeed, the calculated vinyl complexation energy, **IV** → **VIII** + C_2H_3, is only 6.3(6.1) kcal/mol.

In the next step of the reaction, the C−O bond is formed between the carbon atom of the vinyl radical and the O^1 atom of the O^1H-bridge, which is found to occur via transition state **V**. As seen in Figure 6, transition state **V**, TS2, has the geometry

of the "active part" very close to that of intermediate **IV**, and the O^1-CHCH_2 bond that is being formed is calculated to be 2.166(2.150) Å. This indicates that **V** is an early transition state, reflecting the large exothermicity of the step. In **V** there is a weak H-bonded interaction between the vinyl ligand and the right-hand side terminal water with a C···HO distance of 1.988-(2.051) Å, which apparently additionally stabilizes the transition state. The barrier height for the vinyl addition to the hydroxyl ligand calculated relative to the intermediate **IV** is 11.5(9.0) kcal/mol. Obviously, this step of the reaction is not rate-determining and can occur rather fast.

Overcoming the barrier at **V** leads to the vinyl-alcohol complex **VI**. As seen in Figure 6, the structure of this complex for the ^{9}A state is different than that for the ^{11}A state. For the ground state ^{11}A, the formed vinyl alcohol molecule is nearly dissociated from the binuclear Fe-center. On the other hand, for the excited state ^{9}A, there is vinyl alcohol bound as the first shell ligand to Fe^2 with the $Fe^2-O(H)C_2H_3$ bond distance of 2.145 Å. In doing so, one of the "legs" of the bridging carboxylate is dissociated from Fe^2 and H-bonded to the HO bond of vinyl alcohol. These geometrical differences are reflected in the dissociation energy of vinyl alcohol from **VI**, which is calculated to be 3.1(0.9) kcal/mol.

The second pathway of reaction of **I** with the ethylene molecule is the epoxidation mechanism (see Figure 7), which also starts by the coordination of the ethylene molecule to the active site. However, for this pathway to proceed, the ethylene molecule should coordinate to the bridging O^1-center with its C═C double bond. As was discussed above, the coordination of C_2H_4 to the diiron active site gave only one weakly bound prereaction complex **II**, where the ethylene molecule is bound to the O^1-center with one of its H-atoms. Therefore, for the epoxidation reaction to proceed either the ethylene molecule in the complex **II** should rearrange to make its C═C double bond available for O^1-center (may be called isomerization process), or it should dissociate and then recoordinate to the O^1-center with its C═C double bond (called dissociation process). Because both of these processes, isomerization and dissociation, are expected to proceed with very small energetic barriers and not to contribute significantly to the reaction mechanism, below we will not discuss these processes. We will start our discussion from the reactants, **I** and the ethylene molecule, and will bring the ethylene molecule to the O^1-center via its C═C double bond.

Our calculations show that the coordination of the ethylene molecule to O^1 with its C═C double bond leads to formation of the ethylene oxide OC_2H_4 complex **IX**, without barrier. This process is found to be a highly exothermic, by 44.7(62.7) kcal/mol. For the ground ^{11}A state of **IX** the ethylene oxide dissociates to an outer sphere ligand and binds to the Fe−Fe core only with H-bond (not shown in Figure 7), while in the ^{9}A state the OC_2H_4 molecule is bound directly to the Fe^2 center with an $Fe^2-OC_2H_4$ distance of 2.110 Å. One leg of the bridging carboxylate dissociated from the Fe^2-center and formed a H-bonded interaction with the terminal water molecule. Because this epoxidation process starts from the same prereaction complex as the C−H insertion pathway and occurs without barrier (or with a very small dissociation or isomerization barrier), the C−H insertion reaction with its TS1 and TS2 transition states cannot compete with the epoxidation reaction. Therefore, one may conclude that the only product of the reaction of complex **I** with ethylene is the OC_2H_4 molecule. Given the industrial importance of epoxidation reactions, dimetal bridged oxo compounds should be investigated as efficient catalysts for such reactions.

One should note that recently Shaik and co-workers[36] have shown that epoxidation of ethylene by **(**Porp)FeO^+, model of compound **I** in the Fe-heme, also occurs without energetic barrier. In this aspect, models of non-heme and heme Fe proteins behave similarly.

IV. Conclusions

From the discussions given above, we may draw the following conclusions:

(1) The improving basis sets from SBK($+d_{C,O}'$) to SBK-($+d_{C,O}$) and SBK($+d_{C,N,O}$) do not significantly change the calculated energies of the reaction **I** + CH_4. Therefore, we use SBK($+d_{C,O}$) for energy calculations of the intermediates, transition states, and products of the reaction of **I** (model of compound **Q**) with hydrocarbons.

(2) The improvement of the model system to the "medium", **I_m**, did not change our qualitative conclusions made on the basis of the "small" model, **I**, studies, while it significantly changed the calculated energetics.

(3) The H^b-atom abstraction (or C−H bond activation) barrier at transition state **III**, which was previously reported to be a rate-determining step for the entire reaction of compound **I** with the methane molecule, is found to be a few kcal/mol lower for C_2H_6 and CH_3F than for CH_4 substrate. The calculated trend in the H^b-abstraction barrier, CH_4 (21.8 kcal/mol) > CH_3F (18.8 kcal/mol) ≥ C_2H_6 (18.5 kcal/mol), is consistent with the $C-H^b$ bond strength in these substrates. Thus, the weaker the $C-H^b$ bond, the lower is the H^b-abstraction barrier. If the rate-determining barrier of the reaction of **I** is the H^b-atom abstraction step for all these substrates, then one should expect faster kinetics for the ethane rather than for the methane molecule. However, according to experimental studies, the overall kinetics of the reaction of **Q** with methane are faster than any other alkanes reacting with MMO. This suggests that the overall rate-determining step of the reaction of **Q** with ethane and methane molecules is different, and, possibly, the substrate transport to the active site is the rate-determining step of the overall kinetics of the reaction of **Q** with the ethane molecule.

(4) Replacement of a H-atom in a methane molecule with more electronegative groups (or atoms) tends to make the H^b-abstraction transition state less "reactant-like". In contrast, the replacement of the H-atom in CH_4 with less electronegative groups (or atoms) makes the H^b-abstraction transition state more "reactant-like".

(5) The epoxidation of ethylene by compound **Q** is expected to proceed without (or with a very small) barrier and is a highly exothermic process. Considering the existence of a substantial barrier for C−H activation, one can expect that the only product of the reaction of complex **I** (model of **Q**) with ethylene is ethylene oxide, which is consistent with the experiment. Given the industrial importance of epoxidation reactions, it is suggested that diiron bridged oxo compounds could be efficient catalysts for the alkene epoxidation process.

(36) De Visser, S. P.; Ogliaro, F.; Harris, N.; Shaik, S. *J. Am. Chem. Soc.* **2001**, *123*, 3037.

(6) In the present study, the protein environment around the active site is completely neglected. Although the inclusion of the protein environmental effects on the enzyme reactivity is a formidable task, such a study for the structure of the active site has been published.[26] It is likely that soon the reaction at the active site will be studied taking into account the protein environment.

Acknowledgment. The present research is in part supported by a grant (CHE-9627775) from the National Science Foundation. Acknowledgment is made for generous support of computing time at Bar Ilan University Computer Center. Acknowledgment is also made to the Cherry L. Emerson Center of Emory University for the use of its resources, which is in part supported by a National Science Foundation grant (CHE-0079627) and an IBM Shared University Research Award.

Supporting Information Available: Figure S1: The potential energy profile (in kcal/mol) at the B3LYP/SBK(+$d_{C,N,O}$)// B3LYP/SBK level for both the ^{9}A and the ^{11}A state of the methane activation reaction by model compound **Q** for "medium" and "small" models. Table S1: Total and relative energies of various intermediates and transition states, for spin multiplicities of $2S + 1 = 9$ and 11, for the reaction of MMO with methane on the O-side. Table S2: Mulliken atomic spin densities for the various intermediates and transition states of the N-side pathway **I** + methane reaction. Table S3: Cartesian coordinates of all the structures optimized at the B3LYP/SBK level (PDF). This material is available free of charge via the Internet at http://pubs.acs.org.

JA0176393